Solar Energy 247 (2022) 171–176

Contents lists available at ScienceDirect

Solar Energy

journal homepage: www.elsevier.com/locate/solener

21.16%-efficiency p-type TOPCon solar cell with ALD-Al_2O_3/MoO_x/Ag as a hole-selective passivating contact

Hao Cheng [a], Zengguang Huang [a,c,*], Lijuan Zhang [a], Ying Liu [a], Xiaomin Song [a], Rui Tong [b], Sihua Zhong [a], Linxing Shi [a], Xiangyang Kong [d], Wenzhong Shen [d]

[a] School of Science, Jiangsu Ocean University, Lianyungang 222005, Jiangsu Province, PR China
[b] JA Solar, Yangzhou 225131, Jiangsu Province, PR China
[c] Jiangsu Institute of Marine Resources Development, Lianyungang 222005, Jiangsu Province, PR China
[d] School of Physics and Astronomy, School of Materials Science and Engineering, and Institute of Solar Energy, Shanghai Jiao Tong University, Shanghai 200240, PR China

ARTICLE INFO

Keywords:
p-type TOPCon
Hole-selective
Passivating contacts
ALD-Al_2O_3
MoO_x

ABSTRACT

High-performance hole-selective passivating contact is of significance in obtaining the high efficiency of a full-area carriers-selective contact-based solar cell. In this work, we prepared a hole-selective passivating contact of Al_2O_3/MoO_x/Ag and applied it to the rear of the *p*-type tunneling oxide passivated contact (TOPCon) solar cell. It is found that the ultrathin atomic-layer-deposited (ALD) Al_2O_3 as a tunneling layer played an essential role in improving the hole selectivity of Al_2O_3/MoO_x/Ag structures, and the optimal thickness of the tunneling layer Al_2O_3 is ~ 0.56 nm. An ultra-low resistivity of 1.84 mΩ·cm^2 was obtained on the Al_2O_3 (0.56 nm)/MoO_x (7 nm)/Ag (120 nm) structure. Benefiting from the high-performance hole selectivity, the highest efficiency of 21.16% was successfully achieved on the *p*-type TOPCon solar cell, which to our knowledge is the highest efficiency of the MoO_x-based *p*-type TOPCon solar cells. This work demonstrates that the hole-selective passivating contact of Al_2O_3/MoO_x/Ag possesses great potential in the full-area carriers-selective contacts based solar cell.

1. Introduction

Tunneling Oxide Passivated Contact (TOPCon) solar cells with poly-Si (n^+)/SiO_2 structure have been becoming one of the most competitive commercial crystalline silicon (*c*-Si) solar cells (Chen et al., 2020; Glunz et al., 2021; Yu et al., 2021), attributing to the high conversion efficiencies and the high process-compatibility with the baseline of the passivated emitter and rear cells (PERCs). The high output performance of the TOPCon lies in the excellent electron-selectivity properties benefiting from the high level of passivation of tunneling oxide layers and the excellent conductivity of poly-Si (n^+)/SiO_2 (Chandra Mandal et al., 2020; Gao et al., 2019; Khokhar et al., 2021).

However, the poly-Si (n^+)/SiO_2 structure-based TOPCon solar cells suffer from two major limitations. Firstly, the poly-Si (n^+)/SiO_2 structure requires high-temperature processes, including thermal oxidation (~900 ℃) and ~450 ℃ plasma-enhanced chemical vapour deposition (PECVD). Secondly, the poly-Si (n^+) layer has significant parasitic absorption, and thus limits the output performance of the bifacial TOPCon solar cell. To address the issues imposed, wide-bandgap transition metal oxides (TMO) with low parasitic absorption (Gerling et al., 2016b) have attracted many research interests because these thin films can be easily prepared through the low-temperature and simple techniques such as thermal evaporation, atomic layer deposition (ALD), spin coating and magnetron sputtering. Yang et al. (Yang et al., 2016) developed a TiO_2 (~2.5 nm, ALD) film based electron-selective contact, achieving low surface recombination (S_{eff} ~11 cm·s^{-1}) and low contact resistivity (ρ_c ~0.02 mΩ·cm^2) at the silicon and metal interface simultaneously. Wan et al. (Wan et al., 2017) demonstrated a TaO_x (~6 nm, ALD) as an electron-selective contact, resulting in high-quality passivation (J_0 ~22.5 fA/cm^2) and the low contact resistivity (ρ_c ~0.35 mΩ·cm^2) to the silicon surface.

Furthermore, the hole-selective contacts generally exhibit lower selectivity than the electron-selective contacts (Schmidt et al., 2018). Hence, it is necessary to improve the surface passivation and holes conductivity to improve the performances of the hole-selective-contacts-based TOPCon solar cells. Many TMOs can be promising candidates for high-performance hole-selective contacts, such as molybdenum oxide (MoO_x) (Battaglia et al., 2014), nickel oxide (NiO_x) (Hossain et al.,

* Corresponding author at: School of Science, Jiangsu Ocean University, Lianyungang 222005, Jiangsu Province, PR China.
E-mail address: zghuang@jou.edu.cn (Z. Huang).

https://doi.org/10.1016/j.solener.2022.10.019
Received 12 May 2022; Received in revised form 10 July 2022; Accepted 7 October 2022
Available online 23 October 2022

2021), tungsten oxide (WO_x) (Bivour et al., 2015) and vanadium oxide (VO_x) (Gerling et al., 2016a). Among these candidates, molybdenum oxide (MoO_x) is the most widely investigated material due to the wide bandgap (~3 eV) and high work function (WF), leading to an upward band bending at the silicon interface (Messmer et al., 2018). Zhang et al. (Zhang et al., 2018) deposited a 9 nm MoO_x film on top of c-Si by thermal evaporation, achieving a J_0 of 187 fA/cm^2 and a ρ_c of 82.5 mΩ·cm^2. Cao et al. (Cao et al., 2019) studied the heterojunction (SHJ) solar cells with full-area rear MoO_x/Ag (thermal evaporation sequentially) contacts, achieving an efficiency of 18.49%. Nevertheless, MoO_x does not offer sufficient passivation in contact with silicon. Al_2O_3 film is usually deposited on the front of the cell by ALD (Boryło et al., 2016), acting as an antireflection coating and providing passivation (Dobrzański et al., 2014; Drygała et al., 2016; Szindler and Szindler, 2021). ALD ultrathin Al_2O_3 film is promising tunneling for a hole-selective contact because of the excellent chemical and field-effect passivation (Chowdhury et al., 2020; Huang et al., 2015; Leszek et al., 2015; Öğütman et al., 2020). Based on the hole-selective Al_2O_3/MoO_x stack, Sen et al. applied it to the front side of the TOPCon device and achieved an efficiency of 18.2% (Ah Sen et al., 2021). However, the passivation superiority of the tunneling passivation layer Al_2O_3 and the holes conductivity of the Al_2O_3/MoO_x stack were not fully demonstrated.

In this work, an Al_2O_3/MoO_x/Ag structure as the hole-selective contact was prepared on the full-area rear of the *p*-type *c*-Si TOPCon solar cell utilizing low-temperature ALD and thermal evaporation techniques. Firstly, the structural composition of the Al_2O_3/MoO_x stack was represented in the way of transmission electron microscope (TEM) and X-ray photoelectron spectra (XPS), respectively. Secondly, the thickness dependence of the ALD-Al_2O_3 tunneling layer on the passivation effect and the conductivity of the Al_2O_3/MoO_x/Ag structure for holes were investigated. Finally, the optimal Al_2O_3/MoO_x/Ag structure was applied to the full-area rear surface of the *p*-type TOPCon solar cell (53 × 53 mm^2), achieving the highest efficiency of 21.16%, revealing the high hole selectivity of the Al_2O_3/MoO_x/Ag structure.

2. Experimental process

2.1. Al_2O_3/MoO_x stack deposition and device preparation

The device structure consists of a front Ag/SiN_x/SiO_2 contact (Huang et al., 2019) and a rear Al_2O_3/MoO_x/Ag contact. The square (53 × 53 mm^2), boron-doped *p*-type, solar-grade, CZ *c*-Si wafers (⟨1 0 0⟩) acted as substrates, with a thickness of ~180 μm and the resistivity of ~2.0 Ω·cm. The wafers were textured in a NaOH etching solution, followed by the standard cleaning process. Then n^+ emitter was prepared on the front of the wafer by laser-doped $POCl_3$ diffusion in a quartz tube furnace (800 °C) for 40 min. The wafers underwent a smoothing etch to remove the phosphorous silicate glass (PSG). Then, the wafers were cleaned in an RCA 1 & 2 (Kern and Puotinen, 1969) and dipped in the HF (5%) solution to remove the native SiO_x. Then SiO_2 was formed by dry thermal oxidation in a tubular type furnace (850℃), with 8 L/min oxygen flow rate and 0.6 Å/min growth rate. The thicknesses of the SiO_2 were ~1.5 nm. The PECVD-SiN_x layers were deposited to protect the emitter surface by the NH_4/SiH_4 reaction (SC-TD-450C). SiO_2 on the rear of the samples was removed by HF (5%), and the wafers were classified into three groups. The first group (G1) wafers were coated with a thickness of 120 nm Ag layer (full area) by thermal evaporation at the rear. The second group (G2), MoO_3 (~7 nm)/Ag (120 nm) stack was deposited successively at the rear of wafers by thermal evaporation without air break. The third group (G3), the rear side of wafers were grown with the ultrathin Al_2O_3 film (8 cycles) by ALD at 150℃ (the Al_2O_3 growth per cycle is ~0.69 Å), and MoO_3 (~7 nm)/Ag (120 nm full area) were conducted respectively on top of Al_2O_3 by thermal evaporation without air break. Finally, the Ag grids of all group (G1, G2 and G3) cells were screen printed and fired at 800℃ approximately (CF-Series, Despatch). Solar cell structures of G1, G2 and G3 are shown in Fig. 1.

2.2. Characterization

The structure *p*-Si/Al_2O_3/MoO_x/Ag (2 nm/10 nm/120 nm /~180 μm) was prepared. MoO_x (10 nm) and Ag (120 nm) films were deposited respectively by thermal evaporation on a wafer with a single side ALD-Al_2O_3 film (30 cycles, ~2 nm) deposition for TEM (FEI Talos). XPS was utilized to confirm the elemental composition in a vacuum (below 2 × 10^{-9} mbar). The X-ray source is monochromatic Al Kα (h_v = 1486.68 eV) calibrated with the carbon reference. A scanning electron microscope (SEM, Regulus8100, Hitachi, Japan) was used to observe the cross-section of the device and analyze the stack distribution on the back of the device. To investigate the surface passivation performance of Al_2O_3, the quasi-steady-state photoconductance decay tester (Sinton WCT-120) was used to measure the effective minority carrier lifetimes (τ_{eff}) of the samples at the minority carrier concentration of 1 × 10^{15} cm^{-3}. Single-side deposited samples were prepared to measure the contact resistivity (ρ_c) by the transfer length method (TLM). The pad spacing of the shadow mask is 0.15, 0.2, 0.3, 0.4, 0.6 and 0.8 mm, and the electrode width is 3 mm. A MoO_x/Ag (~7 nm/120 nm) stack was thermally evaporated on top of Al_2O_3 by a shadow mask (Liu et al., 2021). The dark current–voltage (I-V) measurements were performed through a four-probe station. External quantum efficiencies (EQEs) of the devices were measured with the platform of quantum efficiency measurement (PV Measurements QEX10). A BERGER Lichttechnik Single Cell Tester investigated I-V characteristics of the solar cells under the AM1.5 illumination (Crown Tech IV Test Station 2000).

3. Results and discussions

3.1. Characterization of Al_2O_3/MoO_x stack

In order to investigate the structural composition of the Al_2O_3/MoO_x stack, the structure of *c*-Si/Al_2O_3/MoO_x/Ag was prepared. Firstly, 30 cycles of ALD Al_2O_3 film were deposited, forming a thickness of ~2 nm.

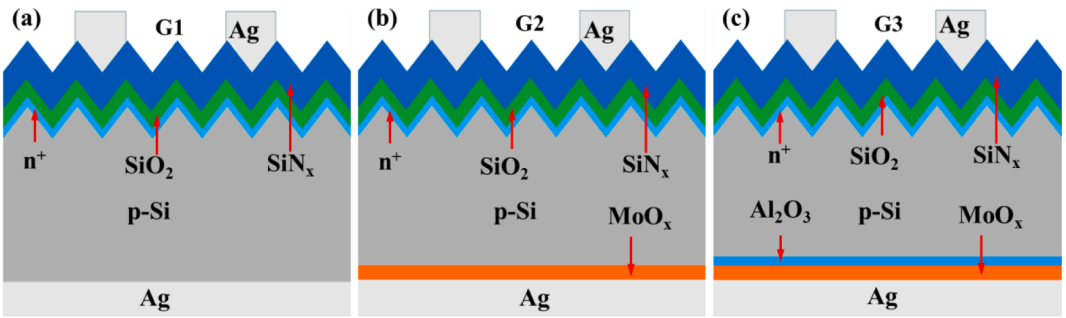

Fig. 1. Solar cell structures for (a) *p*-Si/Ag, (b) *p*-Si/MoO_x/Ag, (c) *p*-Si/Al_2O_3/MoO_x/Ag.

Secondly, after the deposition of the Al_2O_3 film, MoO_x (10 nm) and Ag (120 nm) layers were deposited respectively by thermal evaporation without air break. Fig. 2(a) shows the 50 nm cross-sectional TEM image of the cell's rear surfaces (*c*-Si/Al_2O_3/MoO_x/Ag). The distribution of Al_2O_3/MoO_x stack can be observed clearly in Fig. 2(b), which is verified in Fig. 3. The cross-section of the device under SEM is shown in Fig. 2(c), with a pyramid structure on the front and an Al_2O_3/MoO_x/Ag structure on the back.

The Mo 3d core level energy spectra (see Fig. 3(a)) are divided into the two peaks centred at 232.9 and 231.7 eV, respectively, in line with Mo^{6+} and Mo^{5+} states, oxygen vacancies lead to the appearance of Mo^{5+} cations (Kumar et al., 2021). A defect band caused by oxygen vacancies in the MoO_x aids hole transport between the Si valence band and the MoO_x conduction band in the way of trap-assisted tunneling (Vijayan et al., 2018). These oxygen vacancies increase the conductivity of the MoO_x film, which promotes the accumulation of holes (Ramana et al., 2007). Fig. 3(b) shows the core level O 1 s for MoO_x film with a peak centred 530.5 eV, which corresponds to Mo-O bonding. The atomic ratio of O/Mo is estimated to be 2.68 (<3). As seen in Fig. 3(c), 3(d), the core level spectrum of Al 2p and O 1 s are located at 74.8 eV and 531.6 eV, respectively, which correspond to the Al-O bond in keeping with previous reports about XPS of the Al_2O_3 film (Renault et al., 2002).

3.2. Passivation and conductivity

To demonstrate the surface passivation performance of Al_2O_3, the τ_{eff} of *c*-Si wafers deposited with different thicknesses of Al_2O_3 films was measured (see Fig. 4). As shown in Fig. 4(a), the samples symmetrically coated with thicker Al_2O_3 films (30 cycles and 50 cycles) reach a higher τ_{eff} (30.1 *us*, 18.7 *us*) after annealing at 425℃ than the τ_{eff} (18.2 *us*, 2.8 *us*) of samples without annealing. However, the τ_{eff} of the samples with thinner Al_2O_3 (6 cycles, 8 cycles and 10 cycles) decreases in the high-temperature annealing (200℃, 300℃ and 425℃). The maximum τ_{eff} of the sample with Al_2O_3 (8 cycles) without annealing is 51.7 *us*. Post-deposition annealing improves the lifetime for Al_2O_3 layers (ALD) thicker than 10 ALD cycles, while for Al_2O_3 layers thinner than 10 ALD cycles, annealing causes the thickening of the interlayer, which is likely to form Si-O bonds, resulting in the reduction of τ_{eff} (Ah Sen et al., 2021). The passivation performance of Al_2O_3 with 30 cycles and 50 cycles is improved after high-temperature annealing. However, the thinner Al_2O_3 is suitable for charge carrier tunneling. In terms of ultrathin Al_2O_3 films, due to the increase in interface state density, the passivation quality of the ultrathin Al_2O_3 film deteriorates, which may be caused by the incomplete reaction of trimethyl-aluminium (TMA) molecules in the first ALD cycle (Werner et al., 2011). Nevertheless, attributing to the fixed negative charge, the thinner Al_2O_3 can provide field-effect passivation. Werner et al. introduced the Al_2O_3 passivation layer (1 nm) and obtained low surface recombination (S_{eff} < 100 cm/s), which attributes to the high fixed negative charge of Al_2O_3 film (Werner et al., 2011). The as-deposited ALD is amorphous, consequently no crystallized peaks after deposition. After annealing, it is difficult to assign a phase to each specific peak due to uncertainty about the exact location of the peaks and the presence of several double peaks (Fu, 2021). X-ray diffraction of Al_2O_3 before and after annealing is carried out, and the test

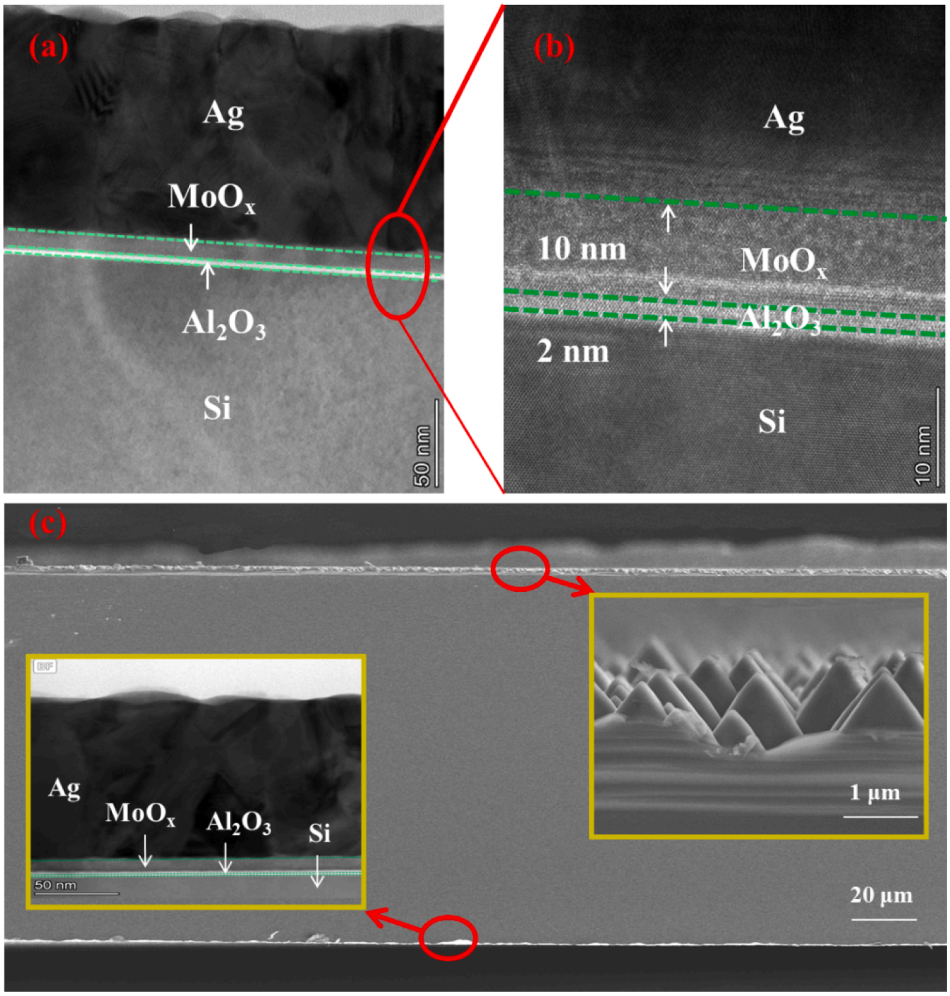

Fig. 2. Cross-sectional view of the *c*-Si/Al_2O_3/MoO_x/Ag structure under TEM (a) 50 nm and (b) 10 nm, (c) cross-sectional view of the device under SEM.

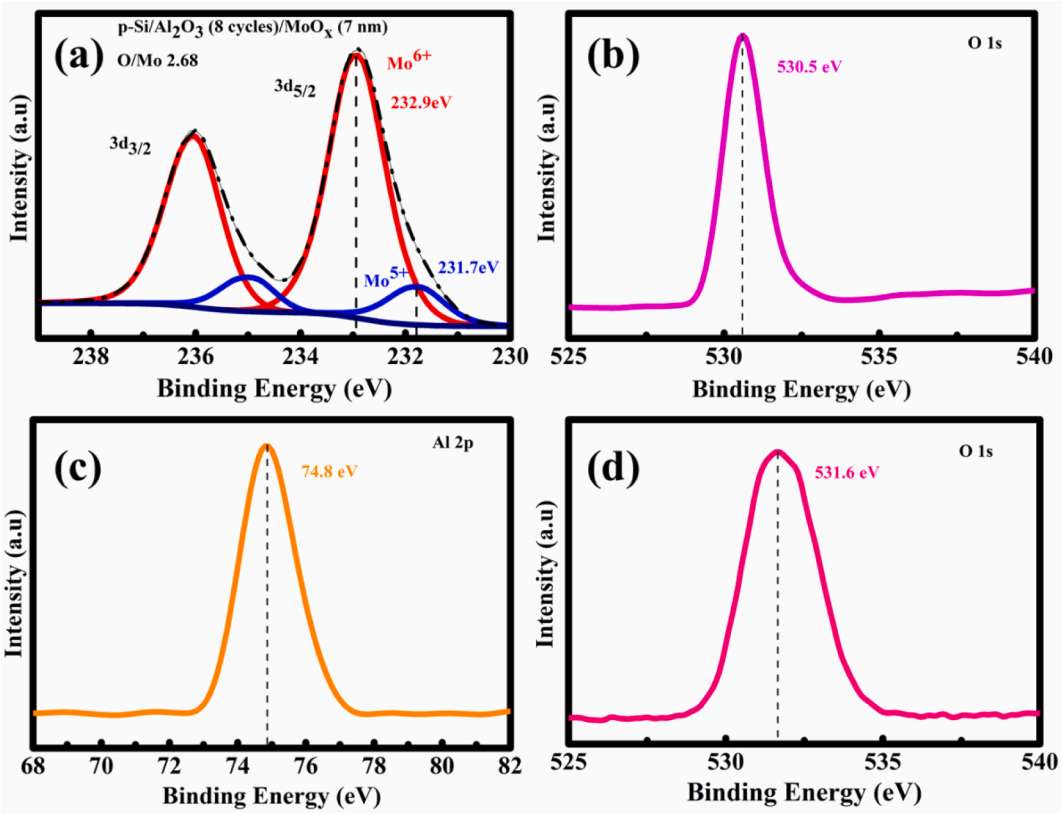

Fig. 3. XPS spectra of (a) Mo 3d (b) O 1 s for MoO_x, (c) Al 2p (d) O 1 s for Al_2O_3.

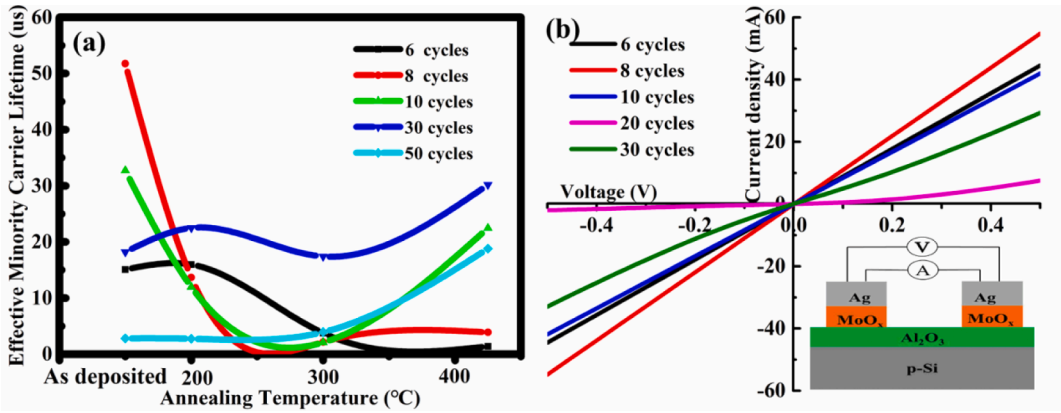

Fig. 4. (a) The function of τ_{eff} at different annealing temperatures with different thicknesses of Al_2O_3, (b) a schematic of TLM and I-V measurement results of Al_2O_3/MoO_x stack with different Al_2O_3 thicknesses.

results are consistent with the reference.

Reducing the contact resistance of the Al_2O_3/MoO_x stack is crucial to implementing ohmic contact with *c*-Si. TLM was used to measure the ρ_c of the stack, and I-V measurement results are exhibited in Fig. 4(b). A MoO_x (~7 nm) film and an Ag (120 nm) film were evaporated on the top of the Al_2O_3 layer to create the $Al_2O_3/MoO_x/Ag$ contact structure by a shadow mask. From the I-V measurements of the different Al_2O_3 thicknesses (the same pad spacing), it is clear that the contacts of the samples with thinner Al_2O_3 (6 cycles, 8 cycles and 10 cycles) showed an ohmic behaviour. After the correlation of the linear fits, the TLM extraction of ρ_c is 3.66 Ω·cm^2, 1.84 Ω·cm^2 and 2.26 Ω·cm^2, respectively. The samples with thicker Al_2O_3 (20 cycles and 30 cycles) showed a Schottky diode behaviour.

3.3. Solar cells

The Al_2O_3/MoO_x stack was applied as a full-area passivation contact to the rear of the *p*-type solar cell due to the excellent passivation and conductivity. The *p*-type solar cells with the rear structure *p*-Si/Ag (G1), *p*-Si/MoO_x/Ag (G2) and *p*-Si/Al_2O_3/MoO_x/Ag (G3) were prepared. The G1 and G2 were used as references. The structured image of G1, G2 and G3 are presented in Fig. 1. The EQE curves of G1, G2 and G3 samples are given in Fig. 5(a). The solar cell with the Al_2O_3/MoO_x stack shows the highest EQE in the wavelength of 500–1100 nm than the devices without Al_2O_3/MoO_x stack, attributing to excellent passivation performance and low contact resistivity of the Al_2O_3/MoO_x stack. Fig. 5(b) shows the current density–voltage (J-V) and power-voltage (P-V) curves of solar cells with the highest efficiency among G1, G2 and G3 samples.

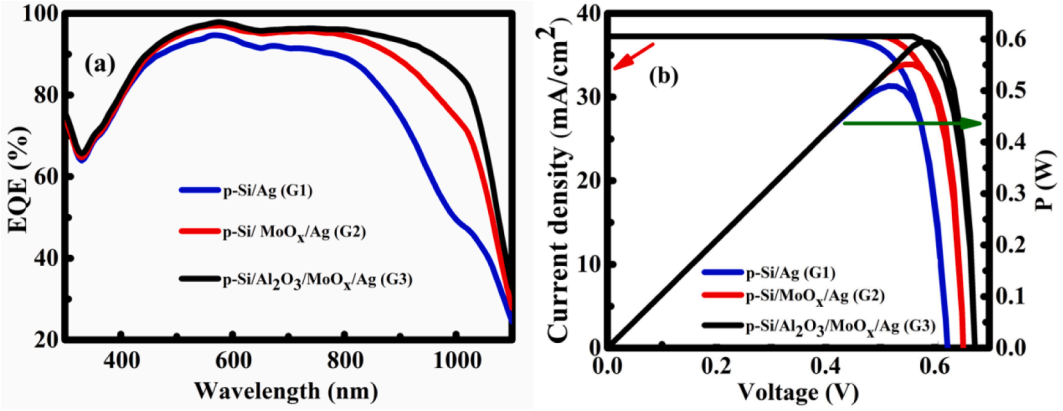

Fig. 5. (a) EQE curves of G1, G2 and G3, (b) J-V, P-V curves of solar cells with the highest efficiency among G1, G2 and G3.

Table 1 shows the specific parameters of the devices in Fig. 5(b). V_{oc} (674 mV) and fill factor *FF* (84.18%) of the device with the Al_2O_3/MoO_x stack are much higher than those without Al_2O_3 films. The fixed negative charge of Al_2O_3 can act as a back surface field and provide passivation. Gerling et al.(Gerling et al., 2016b) found that MoO_x had limited inherent passivation because of the high work function, which decreases the density of surface electrons. In contact with elemental Si, MoO_x is not thermodynamically stable (Hubbard and Schlom, 2011), and thus yields high interface recombination velocities (Sun et al., 2017; Zhang et al., 2018). Al_2O_3/MoO_x stack leads to the V_{oc} increase from 623 mV to 674 mV. In contact with elemental Si, MoO_x leads to an upward band bending because of the high work function, which promotes hole accumulation at the interface and reduces the contact resistivity. Thus, *FF* increases from 77.87% to 80.55%. Meanwhile, the ultrathin Al_2O_3 film acts as a tunneling oxide layer, owing to the negative interface charge density of Al_2O_3, the holes accumulation is further promoted, resulting in the increase of *FF* from 80.55% to 84.18%. The result illustrates that Al_2O_3/MoO_x stack significantly improves the device performance.

Table 2 shows the output parameters of the reference (Cao et al., 2019) and our experiment. Compared to the cells with a full area rear MoO_x/Ag contact fabricated by Cao et al., the device based on Al_2O_3/MoO_x/Ag contact has a V_{oc} increase of 43 mV, and a *FF* increase of 3.3%, consequently increasing η from 18.49% to 21.16% (a relative increase of 14.4%). The improvement in device performance is attributed to the excellent chemistry and field passivation of Al_2O_3 film. More holes are collected by MoO_x films through tunneling oxide layers.

Fig. 6 shows that the solar cell obtained the highest efficiency of 21.16% with a V_{oc} of 674 mV, a J_{sc} of 37.30 mA/cm^2, and a *FF* of 84.18%, whose maximum power is 0.594 W. Compared to the sample without Al_2O_3, V_{oc} and *FF* of the sample with deposited Al_2O_3 were increased by 3% and 4.5%, respectively. Inserting an ultrathin Al_2O_3 between *c*-Si and MoO_x is an effective method to improve the interface passivation and preserve the hole-selective accumulation by suppressing the reaction of *c*-Si/MoO_x (Ah Sen et al., 2021). Finally, attributing to the excellent performance of the Al_2O_3/MoO_x stack in terms of passivation and conductivity, the highest efficiency of 21.16% of the *p*-type TOPCon solar cell with Al_2O_3/MoO_x/Ag is successfully achieved.

Table 1
Comparison of output performances for G1, G2 and G3.

ear structure (53 × 53 mm^2)	V_{oc} (mV)	J_{sc} (mA/cm^2)	*FF* (%)	Highest PCE (%)	Average PCE (%)
p-Si/Ag	623	37.30	77.87	18.11	18.00
p-Si/MoO_x /Ag	652	37.30	80.55	19.60	19.23
p-Si/Al_2O_3 /MoO_x /Ag	674	37.30	84.18	21.16	21.02

Table 2
Comparison of output performances of the device in the Ref.

Rear structure	V_{oc} (mV)	J_{sc} (mA/cm^2)	*FF* (%)	PCE (%)
p-Si/MoO_x/Ag (ref.)	631	36.21	80.89	18.49
p-Si/Al_2O_3/MoO_x/Ag	674	37.30	84.19	21.16

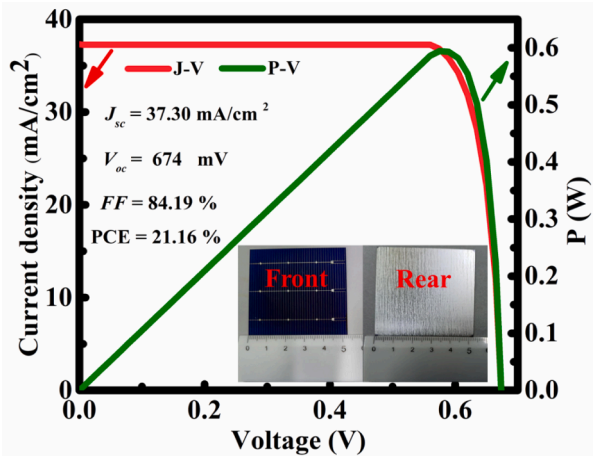

Fig. 6. The J-V and P-V curves of the 21.16% efficiency solar cell with an optimal Al_2O_3 (8 cycles)/MoO_x (7 nm)/Ag structure.

4. Conclusions

This work demonstrates that the ALD-Al_2O_3/MoO_x/Ag structure possesses well hole selectivity for the full-area *p*-type TOPCon solar cell. The result shows that the ultrathin ALD-Al_2O_3 thin film acts as a tunneling layer like an ultrathin SiO_x layer, and plays a vital role in improving the hole selectivity of Al_2O_3/MoO_x/Ag structure. By optimization of the thickness of ALD-Al_2O_3, the highest τ_{eff} of 51.7 *us* and the lowest ρ_c of 1.84 mΩ•cm^2 were simultaneously obtained on the Al_2O_3 (0.56 nm)/MoO_x (7 nm)/Ag (120 nm) structure. Benefiting from the excellent hole selectivity of this structure, we successfully achieved the highest efficiency of 21.16% of MoO_x-based *p*-type TOPCon solar cell, as well as a V_{oc} of 674 mV, a *FF* of 84.18% and a J_{sc} of 37.30 mA/cm^2. The improvement of hole selectivity of the ALD-Al_2O_3/MoO_x/Ag structure demonstrates an effective way to the full passivating contacts high-efficiency crystalline silicon solar cells.

Declaration of Competing Interest

The authors declare that they have no known competing financial

interests or personal relationships that could have appeared to influence the work reported in this paper.

Acknowledgements

This work was supported by the Natural Science Foundation of Jiangsu Province (BK2022 "Study on a novel high-performance Si-based TBC solar cell", BK20221395), the Major projects of the Natural Science Foundation of universities in Jiangsu Province (20KJA430013), the Natural Science Foundation of China (61774069, 62104086, 11834011 and 62034009), the "333" Project of Jiangsu Province, the "Qinglan" Project of Jiangsu Education Department, the Postgraduate Research & Practice Innovation Program of Jiangsu Province (KYCX20_2930, KYCX21_3139), the Postgraduate Research & Practice Innovation Program of Jiangsu Ocean University (KYCX2022-02), Lianyungang Haiyan Plan (2020-QD-010).

References

Ah Sen, M.T.S.K., Bronsveld, P., Weeber, A., 2021. Thermally stable MoO_x hole selective contact with Al_2O_3 interlayer for industrial size silicon solar cells. Sol. Energy Mater. Sol. Cells 230, 111139.

Battaglia, C., de Nicolás, S.M., De Wolf, S., Yin, X., Zheng, M., Ballif, C., Javey, A., 2014. Silicon heterojunction solar cell with passivated hole selective MoO_x contact. Appl. Phys. Lett. 104 (11), 113092 https://doi.org/10.1063/1.4868880.

Bivour, M., Temmler, J., Steinkemper, H., Hermle, M., 2015. Molybdenum and tungsten oxide: high work function wide band gap contact materials for hole selective contacts of silicon solar cells. Sol. Energy Mater. Sol. Cells 142, 34–41. https://doi.org/10.1016/j.solmat.2015.05.031.

Boryło, P., Lukaszkowicz, K., Szindler, M., Kubacki, J., Balin, K., Basiaga, M., Szewczenko, J., 2016. Structure and properties of Al_2O_3 thin films deposited by ALD process. Vacuum 131, 319–326.

Cao, S., Li, J., Lin, Y., Pan, T., Du, G., Zhang, J., Yang, L., Chen, X., Lu, L., Min, N., Yin, M., Li, D., 2019. Interfacial behavior and stability analysis of p-type crystalline silicon solar cells based on hole-selective MoO_x/metal contacts. Solar RRL 3, 1900274. https://doi.org/10.1002/solr.201900274.

Chandra Mandal, N., Biswas, S., Acharya, S., Panda, T., Sadhukhan, S., Sharma, J.R., Nandi, A., Bose, S., Kole, A., Das, G., Maity, S., Chaudhuri, P., Saha, H., 2020. Study of the properties of SiO_x layers prepared by different techniques for rear side passivation in TOPCon solar cells. Mater. Sci. Semicond Process. 119, 105163 https://doi.org/10.1016/j.mssp.2020.105163.

Chen, D., Chen, Y., Wang, Z., Gong, J., Liu, C., Zou, Y., He, Y., Wang, Y., Yuan, L., Lin, W., Xia, R., Yin, L., Zhang, X., Xu, G., Yang, Y., Shen, H., Feng, Z., Altermatt, P. P., Verlinden, P.J., 2020. 24.58% total area efficiency of screen-printed, large area industrial silicon solar cells with the tunnel oxide passivated contacts (i-TOPCon) design. Sol. Energy Mater. Sol. Cells 206, 110258. https://doi.org/10.1016/j.solmat.2019.110258.

Chowdhury, S., Chavan, G., Kim, S., Oh, D., Kim, Y., Chel Cho, E., Cho, Y., Yi, J., 2020. Analysis of passivation property using thin Al_2O_3 layer and simulation for realization of high-efficiency TOPCon cell. Infrared Phys. Technol. 110, 103436 https://doi.org/10.1016/j.infrared.2020.103436.

Dobrzański, L., Szindler, M., Drygała, A., Szindler, M., 2014. Silicon solar cells with Al_2O_3 antireflection coating. Cent. Eur. J. Phys. 12, 666–670. https://doi.org/10.2478/s11534-014-0500-9.

Drygała, A., Dobrzański, L.A., Szindler, M., Szindler, M.M., Prokopiuk vel Prokopowicz, M., Jonda, E., 2016. Influence of laser texturization surface and atomic layer deposition on optical properties of polycrystalline silicon. Int. J. Hydrogen Energy 41 (18), 7563–7567.

Fu, Z., 2021. Effect of atomic layer deposited Al_2O_3 and subsequent annealing on the nanomechanical properties on various substrates. J. Mater. Sci. 56, 7879–7888. https://doi.org/10.1007/s10853-021-05804-6.

Gao, T., Yang, Q., Guo, X., Huang, Y., Zhang, Z., Wang, Z., Liao, M., Shou, C., Zeng, Y., Yan, B., Hou, G., Zhang, X., Zhao, Y., Ye, J., 2019. An industrially viable TOPCon structure with both ultra-thin SiO_x and n^+-poly-Si processed by PECVD for p-type c-Si solar cells. Sol. Energy Mater. Sol. Cells 200, 109926. https://doi.org/10.1016/j.solmat.2019.109926.

Gerling, L.G., Mahato, S., Morales-Vilches, A., Masmitja, G., Ortega, P., Voz, C., Alcubilla, R., Puigdollers, J., 2016a. Transition metal oxides as hole-selective contacts in silicon heterojunctions solar cells. Sol. Energy Mater. Sol. Cells 145, 109–115. https://doi.org/10.1016/j.solmat.2015.08.028.

Gerling, L.G., Voz, C., Alcubilla, R., Puigdollers, J., 2016b. Origin of passivation in hole-selective transition metal oxides for crystalline silicon heterojunction solar cells. J. Mater. Res. 32, 260–268. https://doi.org/10.1557/jmr.2016.453.

Glunz, S.W., Steinhauser, B., Polzin, J.I., Luderer, C., Grübel, B., Niewelt, T., Okasha, A. M.O.M., Bories, M., Nagel, H., Krieg, K., Feldmann, F., Richter, A., Bivour, M., Hermle, M., 2021. Silicon-based passivating contacts: the TOPCon route. Prog. Photovoltaics Res. Appli. 1–19 https://doi.org/10.1002/pip.3522.

Hossain, M.A., Zhang, T., Zakaria, Y., Lambert, D., Burr, P., Rashkeev, S., Abdallah, A., Hoex, B., 2021. Doped nickel oxide carrier-selective contact for silicon solar cells. IEEE J. Photovolt. 11, 1176–1187. https://doi.org/10.1109/jphotov.2021.3095458.

Huang, Z., Zhong, S., Hua, X., Lin, X., Kong, X., Dai, N., Shen, W., 2015. An effective way to simultaneous realization of excellent optical and electrical performance in large-scale Si nano/microstructures. Prog. Photovoltaics Res. Appl. 23, 964–972. https://doi.org/10.1002/pip.2506.

Huang, Z.G., Gao, K., Wang, X.G., Xu, C., Song, X.M., Shi, L.X., Zhang, Y., Hoex, B., Shen, W.Z., 2019. Large-area MACE Si nano-inverted-pyramids for PERC solar cell application. Sol. Energy 188, 300–304. https://doi.org/10.1016/j.solener.2019.06.015.

Hubbard, K.J., Schlom, D.G., 2011. Thermodynamic stability of binary oxides in contact with silicon. J. Mater. Res. 11, 2757–2776. https://doi.org/10.1557/jmr.1996.0350.

Kern, W., Puotinen, D.A., 1969. Cleaning solution based on hydrogen peroxide for use in silicon semiconductor technology. RCA Rev. 31, 187. https://doi.org/10.1029/RS005i012p01489.

Khokhar, M.Q., Chowdhury, S., Pham, D.P., Hussain, S.Q., Cho, E.-C., Yi, J., 2021. Improving passivation properties using a nano-crystalline silicon oxide layer for high-efficiency TOPCon cells. Infrared Phys. Technol. 115, 103723 https://doi.org/10.1016/j.infrared.2021.103723.

Kumar, M., Cho, E.-C., Prodanov, M.F., Kang, C., Srivastava, A.K., Yi, J., 2021. MoO_x work function, interface structure, and thermal stability analysis of ITO/MoO_x/a-Si (i) stacks for hole-selective silicon heterojunction solar cells. Appl. Surf. Sci. 553, 149552 https://doi.org/10.1016/j.apsusc.2021.149552.

Leszek, A.D., Marek, S., Magdalena, S., Barbara, H., Sonia, K., 2015. The impact of atomic layer deposition technological parameters on optical properties and morphology of Al_2O_3 thin films. OpT. Appl. XLV. No.4. https://doi.org/10.5277/oa150412.

Liu, Y., Sang, B., Hossain, M.A., Gao, K., Cheng, H., Song, X., Zhong, S., Shi, L., Shen, W., Hoex, B., Huang, Z., 2021. A novel passivating electron contact for high-performance silicon solar cells by ALD Al-doped TiO_2. Sol. Energy 228, 531–539. https://doi.org/10.1016/j.solener.2021.09.083.

Messmer, C., Bivour, M., Schön, J., Hermle, M., 2018. Requirements for efficient hole extraction in transition metal oxide-based silicon heterojunction solar cells. J. App. Phys. 124 (8), 085702 https://doi.org/10.1063/1.5045250.

Öğütman, K., Iqbal, N., Gregory, G., Li, M., Haslinger, M., Cornagliotti, E., Schoenfeld, W. V., John, J., Davis, K.O., 2020. Spatial atomic layer deposition of aluminum oxide as a passivating hole contact for silicon solar cells. phys. status solidi (a) 217, 2000348. https://doi.org/10.1002/pssa.202000348.

Ramana, C.V., Atuchin, V.V., Kesler, V.G., Kochubey, V.A., Pokrovsky, L.D., Shutthanandan, V., Becker, U., Ewing, R.C., 2007. Growth and surface characterization of sputter-deposited molybdenum oxide thin films. Appl. Surf. Sci. 253, 5368–5374. https://doi.org/10.1016/j.apsusc.2006.12.012.

Renault, O., Gosset, L.G., Rouchon, D., Ermolieff, A., 2002. Angle-resolved x-ray photoelectron spectroscopy of ultrathin Al_2O_3 films grown by atomic layer deposition. J. Vac. Sci. Technol. A: Vacuum, Surfaces, and Films 20, 1867. https://doi.org/10.1116/1.1507330.

Schmidt, J., Peibst, R., Brendel, R., 2018. Surface passivation of crystalline silicon solar cells: Present and future. Sol. Energy Mater. Sol. Cells 187, 39–54. https://doi.org/10.1016/j.solmat.2018.06.047.

Sun, T., Wang, R., Liu, R., Wu, C., Zhong, Y., Liu, Y., Wang, Y., Han, Y., Xia, Z., Zou, Y., Song, T., Koch, N., Duhm, S., Sun, B., 2017. Investigation of MoO_x/n-Si strong inversion layer interfaces via dopant-free heterocontact. phys. status solidi RRL 11, 1700107. https://doi.org/10.1002/pssr.201700107.

Szindler, M., Szindler, M.M., 2021. Effect of heat treat on the surface morphology and optical properties of the Al_2O_3 thin film for use in solar cells. Opto-Electron. Rev. 29, 181–186. https://doi.org/10.24425/opelre.2021.139602.

Vijayan, R.A., Essig, S., Wolf, S.D., Ramanathan, B.G., Loper, P., Ballif, C., Varadharajaperumal, M., 2018. Hole-collection mechanism in passivating metal-oxide contacts on Si solar cells: insights from numerical simulations. IEEE J. Photovol. 8, 473–482. https://doi.org/10.1109/JPHOTOV.2018.2796131.

Wan, Y., Karuturi, S.K., Samundsett, C., Bullock, J., Hettick, M., Yan, D., Peng, J., Narangari, P.R., Mokkapati, S., Tan, H.H., Jagadish, C., Javey, A., Cuevas, A., 2017. Tantalum oxide electron-selective heterocontacts for silicon photovoltaics and photoelectrochemical water reduction. ACS Energy Lett. 3, 125–131. https://doi.org/10.1021/acsenergylett.7b01153.

Werner, F., Veith, B., Zielke, D., Kühnemund, L., Tegenkamp, C., Seibt, M., Brendel, R., Schmidt, J., 2011. Electronic and chemical properties of the c-Si/Al_2O_3 interface. J. Appl. Phys. 109 (11), 113701 https://doi.org/10.1063/1.3587227.

Yang, X., Bi, Q., Ali, H., Davis, K., Schoenfeld, W.V., Weber, K., 2016. High-Performance TiO_2 -based electron-selective contacts for crystalline silicon solar cells. Adv. Mater. 28, 5891–5897. https://doi.org/10.1002/adma.201600926.

Yu, B., Shi, J., Li, F., Wang, H., Pang, L., Liu, K., Zhang, D., Wu, C., Liu, Y., Chen, J., Lu, W., Cong, R., Yu, W., 2021. Selective tunnel oxide passivated contact on the emitter of large-size n-type TOPCon bifacial solar cells. J. Alloys and Compd. 870, 159679 https://doi.org/10.1016/j.jallcom.2021.159679.

Zhang, T., Lee, C.-Y., Wan, Y., Lim, S., Hoex, B., 2018. Investigation of the thermal stability of MoO_x as hole-selective contacts for Si solar cells. J. Appl. Phys. 124 (7), 073106 https://doi.org/10.1063/1.5041774.